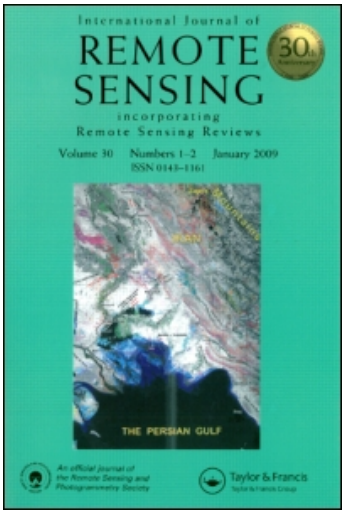

International Journal of Remote Sensing
Publication details, including instructions for authors and subscription information:
http://www.informaworld.com/smpp/title~content=t713722504

A computationally efficient inverse modelling approach of inherent optical properties for a remote sensing model

Vijay Garg[a]; Indrajeet Chaubey[b]
[a] Department of Biological and Agricultural Engineering, University of Arkansas, Fayetteville, AR, USA [b] Department of Agricultural and Biological Engineering, and Department of Earth and Atmospheric Sciences, Purdue University, West Lafayette, IN, USA

Online publication date: 13 September 2010

To cite this Article Garg, Vijay and Chaubey, Indrajeet(2010) 'A computationally efficient inverse modelling approach of inherent optical properties for a remote sensing model', International Journal of Remote Sensing, 31: 16, 4349 — 4371
To link to this Article: DOI: 10.1080/01431160903258225
URL: http://dx.doi.org/10.1080/01431160903258225

International Journal of Remote Sensing
Vol. 31, No. 16, 20 August 2010, 4349–4371

Taylor & Francis
Taylor & Francis Group

A computationally efficient inverse modelling approach of inherent optical properties for a remote sensing model

VIJAY GARG† and INDRAJEET CHAUBEY*‡
†Department of Biological and Agricultural Engineering, University of Arkansas, Fayetteville, AR 72701, USA
‡Department of Agricultural and Biological Engineering, and Department of Earth and Atmospheric Sciences, Purdue University, West Lafayette, IN 47906, USA

(*Received 18 February 2008; in final form 2 November 2008*)

Inverse modelling of inherent optical properties (IOP) is an alternative to the *in situ* measurements of IOP requiring specialized instruments. However, inverse modelling using Monte Carlo models may require very large computational time due to a large number of dynamic model runs needed to search the optimum parameter values. We present a new approach to reduce this computational time. Mathematical relationships were developed for wavelength and concentration dependence of IOP values of suspended mineral based on four parameters. Optimal values of these four parameters were calculated by minimizing the mean sum of error between the physical hyperspectral optical-Monte Carlo (PHO-MC) model predicted reflectance to measured reflectance values for selected 33 reflectance measurements for a set of 11 wavelengths and three suspended sediment concentrations. The computation time was significantly reduced by several orders of magnitude by: (1) replacing the PHO-MC model with 11 wavelengths specific pseudo-simulator models developed by applying artificial neural network approach; and (2) using a nondominated sorted genetic algorithm –II (NSGA II) to search the global optimal solution of four parameters of IOP equations. Determined IOP values of suspended minerals were then successfully validated by using them as input to PHO-MC model to predict reflectance values for an independent set of 287 combinations of 41 wavelengths and seven suspended sediment concentrations.

1. Introduction

Methods used for water quality assessment using remote sensing range from empirical models to physical models. In empirical models, a direct relationship is developed between a data set of measured reflectance values and corresponding optically active constituent (OAC) concentrations using statistical or neural network techniques (Keiner and Yan 1998, Baruah 2000, Panda *et al.* 2004). In physical models, light interaction with water and its OAC is solved in the framework of radiative transfer theory to calculate reflectance either leaving water surface or at some depth of water. Light interaction with water and its OAC is determined based on inherent optical properties (IOP) of each OAC.

Two approaches, namely deterministic and stochastic Monte Carlo, are used to solve radiative transfer of energy (RTE) (Gimond 2002). Mathematical solutions of

*Corresponding author. Email: ichaubey@purdue.edu

International Journal of Remote Sensing
ISSN 0143-1161 print/ISSN 1366-5901 online
http://www.tandf.co.uk/journals
DOI: 10.1080/01431160903258225

deterministic models are difficult to develop and solve because of the complex nature of the interactions between electromagnetic radiation and the various characteristics of the medium. Assumptions, such as ignoring multiple scattering and infinite extents of water body, are made to simplify the solution of the mathematical models. In contrast, Monte Carlo models are conceptually simple, instructive, simple to program, flexible for any geometrical situation and can be used even when boundary conditions and water constituent vary in all three spatial dimensions (Mobley 1994, Doyle and Rief 1998). However, Monte Carlo models are computationally inefficient and running a model can be time-consuming, especially when large numbers of runs are required.

In physical modelling, model structure and the input to model, i.e. IOP values of OAC of water and boundary conditions, determine model prediction accuracy. Knowledge of the IOPs of OAC is still considered insufficient (Yacobi *et al.* 1995, Morel and Maritorena 2001). Furthermore, there exists a large regional and temporal variability by more than an order of magnitude in the IOPs of OAC, such as suspended matter due to their variation in shape, size and composition (Sathyendranath *et al.* 1987, Hoepffner and Sathyendranath 1993, Ciotti *et al.* 2002, Cota *et al.* 2003, Lee and Carder 2004). These IOP values, specific to OAC of a water body, are determined either using the direct *in situ* measurements or by inverse modelling.

Many commercially available instruments such as AC-9 (WetLabs, Inc., Philomath, OR), Hydroscat-6 (HobiLabs, Inc., Bellevue, WA) and a-βeta (HobiLabs, Inc.) have been reportedly used for direct *in situ* measurements of IOPs (Stramska *et al.* 2000, Babin and Stramski 2002). But measurement of IOP in a full-scale experiment is not only expensive and time-consuming but also presents technical difficulties. The accuracy of scattering measurements by instruments are affected by a variety of factors, such as, radiometric calibration; sensor-response function and optical geometry (involving the scattering volume, illumination beam, detection of scattered light and path length in the water); proper angular resolution; temperature, and pressure effects; as well as optical and mechanical imperfections of the instruments (Stramski *et al.* 2004). Thus, a multitude of factors affecting the measurements by available instruments require investigation of alternative methods for accurate IOP determination. Furthermore, the use of *in situ* determined IOP values may not work well within the model prediction due to these errors in the measurements and the inheritance assumption of the model development. Inverse modelling, by employing a remote sensing model and measured concentrations of OAC of water body has been attempted in an effort to overcome the difficulties faced during *in situ* measurements. Inverse modelled IOP value calculations based on algorithms tuned to match the optical properties of local OAC and model structure may improve the accuracy of remote sensing of water quality (Sathyendranath *et al.* 2001). In recent years, inverse modelling of IOP and their use in the model for water quality prediction has received much attention as is evident by a number of studies (e.g. Gordon and Boynton 1997, Barnard *et al.* 1999, Loisel and Stramski 2000, Stramska *et al.* 2000, Loisel *et al.* 2001, Stramski *et al.* 2001, 2004, Babin and Stramski 2002, 2004, Risovic 2002, Babin *et al.* 2003, Cota *et al.* 2003, McKee *et al.* 2003).

Inverse modelling optimizes the number of parameters of the conceptual mathematical formulation of the IOP values of the OAC. These conceptual mathematical formulations account for the variation of IOP due to its concentration and the wavelength of the interacting electromagnetic radiation. However, searching the entire parameter space of the possible solutions to find optimum parameter values

requires a large run of the remote sensing model. Thus, inverse modelling of IOPs using a computationally inefficient Monte Carlo model may need years of computation time. Therefore, most of the inversion models have used semi-analytic remote sensing models (table 1) (Barnard *et al.* 1999, Stramska *et al.* 2000, Loisel *et al.* 2001, Lee *et al.* 2002, Hamre *et al.* 2003, McKee *et al.* 2003), which are basically a simple approximation of the radiative transfer equations (RTEs) first developed by Morel and Prieur (1977).

The objectives of this study were to calculate the suspended mineral particle IOP values by inverse modelling approach using a physical hyperspectral optical-Monte Carlo model (PHO-MC) of Garg *et al.* (2009) and validate them by comparing model predicted reflectance (using estimated IOP values) with the measured reflectance in 400 to 800 nm wavelength range and commonly found suspended mineral particle concentrations in a control water tank study. In this paper, we test the hypothesis that the computation time to determine wavelength specific IOP values using an inverse modelling approach can be reduced by replacing the original model with a computationally efficient pseudo-simulator remote sensing model based on artificial neural network (ANN). Further we test the hypothesis that the optimized solutions of IOPs can be obtained using evolutionary approach based genetic algorithm (GA) as an optimization technique to search the optimal solution of the IOP values. The IOP values thus obtained can be validated by predicting the reflectance based on these IOP values and comparing it with the measured reflectance.

Table 1. Commonly used simplified solutions of the radiative transfer equation.

Equation developed	Parameters	Reference
$R(\lambda,0) = f\dfrac{b_b(\lambda)}{a(\lambda)}$	f varying with sun angle, with a mean value of 0.33; $b_b(\lambda)$ is backscattering coefficient, and $a(\lambda)$ is the absorption coefficient; and $R(\lambda,0)$ is the remote sensing reflectance at surface of the water for λ wavelength	Morel and Prieur (1977)
$R(\lambda,0) = f'\dfrac{b_b(\lambda)}{a(\lambda)+b_b(\lambda)}$	f' varying from 0.324 for a zenith Sun to 0.369 for a uniform sky	Gordon *et al.* (1975)
$R(\lambda,0) = (0.975 - 0.629\mu_0)\dfrac{b_b(\lambda)}{a(\lambda)}$	μ_0 is the cosine of the angle of stream of photons within the water	Kirk (1984)
$R(\lambda,0) = \dfrac{r_d\bar{\mu}_u}{\bar{\mu}_u+\bar{\mu}_d}\dfrac{b_b}{a+kb_b}$ $k = \dfrac{r_d\bar{\mu}_u + r_u\bar{\mu}_d}{\bar{\mu}_u+\bar{\mu}_d}$	r_d represents the mean upward scattering coefficient of the downward traveling photons, while r_u represents the mean downward scattering coefficient of the upward travelling photons, both coefficient normalized with the backward scattering coefficient; upwelling average cosine $\bar{\mu}_u$ is the ratio of upwelling plane irradiance to upwelling scalar irradiance; downwelling average cosine $\bar{\mu}_d$ is the ratio of downwelling plane irradiance to downwelling scalar irradiance	Aas (1987)

This approach was evaluated in a water tank study. Suspended mineral particles, a major contributor to poor water quality for both inland and coastal waters and a major OAC of water, were used in this study. The contribution of suspended mineral particles to remote sensing signals is quite significant as their scattering (Wozniak and Stramski 2004) and absorption (Babin and Stramski 2004, Stramski *et al.* 2004) of light is greater compared with other OAC in water. Also, absorption of light by mineral particles is found to vary by more than an order of magnitude depending upon the shape, size and origin of mineral particles (Babin and Stramski 2004). Similarly, specific backscattering coefficients of suspended matter range from 0.02 to 0.10 $m^2\ g^{-1}$ based on compilations from three different studies by Arst (2003). Very limited quantitative information about these suspended mineral particles is available (Babin *et al.* 2003, Stramski *et al.* 2004), and their contribution to scattering and absorption is poorly known (Babin and Stramski 2004). A computational efficient approach for inverse modelling of IOP can be a useful tool for using remote sensing model to determine wavelength specific reflectance and water quality of a water body.

2. Materials and methods

2.1 *Description of the Physical Hyperspectral Optical – Monte Carlo model*

The PHO-MC model developed by Garg (2006) was used to develop the inverse modelling approach of IOP determination. The model is described here only briefly and an interested reader should consult Garg (2006) and Garg *et al.* (2009) for further details about the model. It should be noted that the PHO-MC model is used here only as a candidate model to illustrate the inverse modelling approach of IOP determination; the methodology developed in this study should be applicable to any remote sensing model.

The PHO-MC model is based on the Monte Carlo solution of the time independent, monochromatic RTE in one spatial dimension (Mobley *et al.* 1993, Mobley 1994):

$$\mu \frac{\mathrm{d}L(z;\xi;\lambda)}{\mathrm{d}z} = -c(z;\lambda)L(z;\xi;\lambda) + \iint_{\xi\in\Xi} L(z;\xi';\lambda)\beta(z;\xi'\rightarrow\xi;\lambda)\mathrm{d}\Omega(\xi') + S(z;\xi;\lambda), \quad (1)$$

where $L(z;\ \xi;\ \lambda)$ is the unpolarized spectral radiance at wavelength λ, depth z and in direction $\xi = (\theta,\phi)$; c is the total attenuation coefficient; β is the volume scattering function and S is the internal source of radiance. To solve equation (1) within a water body, it is necessary to specify: (a) the IOP of the water body, c and β; (b) the distribution of internal sources S radiance (such as bioluminescence); (c) the radiance distribution that is externally incident upon the boundaries of the water body and (d) the physical nature of the boundaries themselves (Mobley *et al.* 1993). PHO-MC model calculates apparent optical properties (AOP) such as remote sensing reflectance $R(\lambda)$, angular fluxes, radiance and irradiance by tracing the probabilistic path of sufficiently large number of photon packets. Photon packet propagation instead of a single photon is used to improve the accuracy of Monte Carlo simulations (Prahl *et al.* 1989, Mobley 1994). Photon packet tracings start immediately before their entry into

the water body and continue until photon packet is either completely absorbed or partially escaped through the air-water interface.

To generate a hyperspectral graph of AOP of an aquatic medium, the model is run for photon packets of different wavelengths. The model divides the water body into many parallel layers to account for IOP depth variation. Optical properties are allowed to change from one layer to another, but within each layer the properties are assumed to be uniform. Horizontal extent of each layer is considered infinite. Water body is considered of infinite horizontal extent, free from bubbles, with a flat water surface. The bottom of water body is considered a Lambertian reflecting surface whose reflectance property is an input in the model. The scattering is assumed elastic.

Initial photon movement direction is decided based on its chances of being from direct light or diffuse light. Measured ratio of diffuse light to the total light provides probabilistic chance of photon packet light source. Before photon packet entry into the water surface, its weight is reduced by the amount of specular reflection calculated using Fresnel law. Photon packet direction of transmission in water is changed from direction of air based on Snell's law. Instead of a photon packet's fixed incremental distance propagation, a varying step size is used according to the method discussed by Mobley (1994) to reduce the statistical noise associated with the Monte Carlo (MC) simulations. Before advancing photon packet to calculated distance, it is first determined if the photon packet remained in the current layer or crossed its upper or lower boundary. If it is found that the photon packet could cross the upper boundary of the layer, it is considered to have reached the air-water interface in the case of the uppermost layer. From the air-water interface, the photon packet is either reflected back or escaped into the air. If the angle of incidence exceeded the critical angle, the photon packet is reflected back fully, otherwise, reflection chance is calculated using Fresnel reflection coefficient. If the photon packet is fully reflected, its path in the body of water in new direction of propagation is traced. Conversely, if a photon packet escapes water surface, its weight, direction and coordinates of point of escape are recorded and tracing of its trajectory is terminated.

If the photon packet is found to cross the lower boundary of the layer, it is moved to the bottom surface of the tank in the case of lowest layer. If the photon packet reached bottom of the tank, its weight is reduced according to the reflectivity of the bottom surface. If the photon packet is found to cross any of the intermediate layers (other than the top and bottom), it is moved the rest of its modified distance in the new layer calculated based on the IOP properties of both layers. If the photon packet remained within a layer, it is moved the required distance.

After each movement, the photon packet is split into two parts; one fraction is absorbed and the rest scattered. The absorbed part of the photon packet is recorded for that location. The photon packet weight is then updated with scattering part. For the scattered fraction, new direction of propagation is decided using Henyey-Greenstien phase function (Prahl *et al.* 1989, Mobley 1994, Gjerstad *et al.* 2003). A new step size is calculated and the photon moved in the new direction as per the above processes. This process continues until the photon packet is terminated. The termination of the photon packet occurs if it was transmitted out of the water surface or if its weight dropped below a threshold value. The model has been shown to simulate reflectance of clear water body accurately (figure 1) (Garg *et al.* 2009).

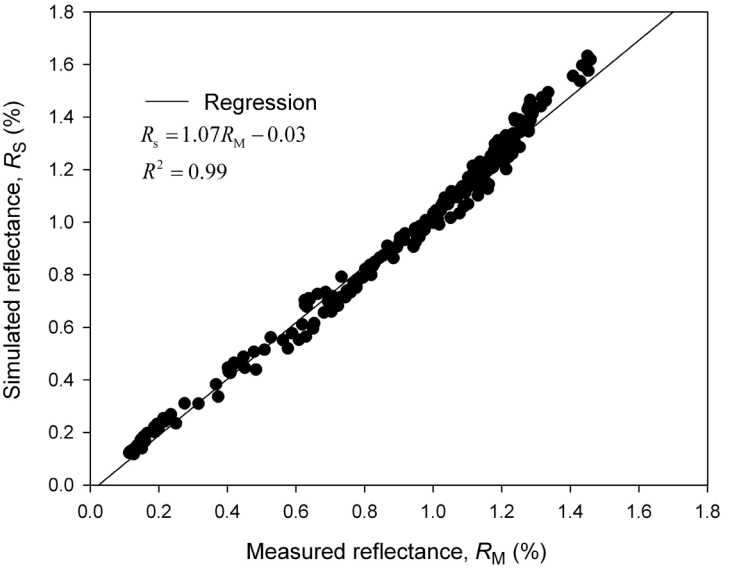

Figure 1. PHO-MC model simulated reflectance (R_S) versus measured reflectance (R_M) of the clear water surface in a tank study for 246 combinations of six water depths (0.75 m, 0.60 m, 0.50 m, 0.40 m, 0.20 m and 0.10 m) and 41 wavelengths (10 nm apart, in the range of 400–800 nm).

2.2 *Experimental data used in inverse modelling*

Remote sensing measurements were conducted at the Arkansas Agricultural Research and Extension Center (36:05:46.8N, 94:10:28.5W, 1294 ft NAVD88), an agricultural station of the University of Arkansas, during 17–18 October 2003, under clear sky conditions. The experimental set-up consisted of a circular vinyl tank (1.67 m in diameter and 0.80 m in height). The tank was located in an open field at the experimental site. The tank bottom and side walls were painted black to eliminate extraneous internal reflections as suggested by McCluney (1976). The tank was filled with clear tap water to 0.75 m depth, with a total volume of 1642 litres. This depth was maintained throughout the experiment. Figure 2 shows the schematic diagram of the experimental setup used to collect reflectance data used in this study. Observations were recorded when the water surface was smooth to avoid effect of wind on the reflectance. All data collection occurred between 13:00 and 15:00, local daylight saving time. Sun zenith angle was obtained for the date, time and location of the experiment from US Naval Observatory Astronomical applications department's website (http://aa.usno.navy.mil/ accessed on 10 May 2006). The value of the Sun's zenith angle varied from 42.3° to 28.0° for the experiments reported here. The refractive index of air was assumed as 1.000. The refractive index of water at different wavelengths was adapted from Mobley (1994) and varied from 1.344 to 1.331, over the 400 nm to 700 nm wavelength range at 10°C for freshwater. For wavelengths beyond 700 nm, the water refractive index was assumed to be equal to its value at 700 nm.

Tap water was used in the experiment. Tap water turbidity was low (0.09 Nephelometric Turbidity Unit), therefore, its IOP values were assumed to be the same as those of the IOPs of pure water. An Analytical Spectral Devices (ASD) FieldSpec Pro Dual VNIR spectroradiometer (Analytical Spectral Devices, Boulder, CO) was used to collect radiance upwelling from the tank. This instrument acquired data in 512 discrete,

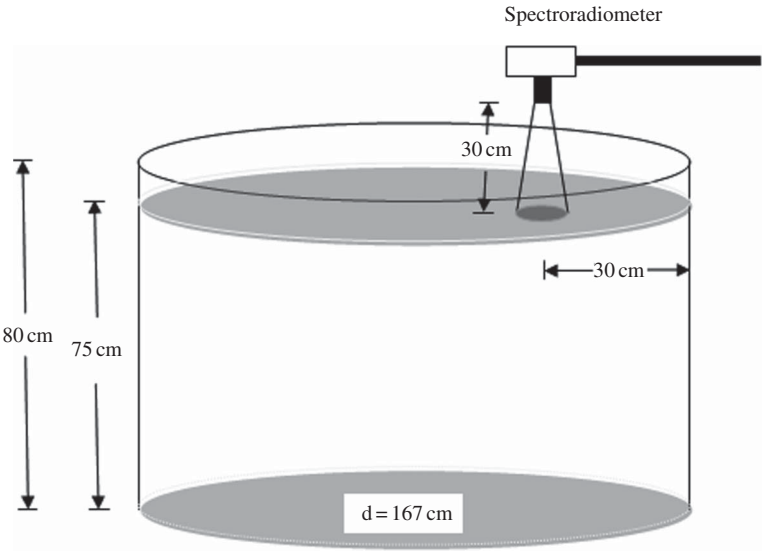

Figure 2. Schematic diagram of the experimental setup to collect reflectance data used in the inverse modeling.

contiguous spectral bands, each of bandwidth 1.438 nm, spread over the spectral range of 336 to 1071 nm. For this study, data from 400 to 800 nm (232 channels) only were used. The instrument had two sensors (target sensor and reference sensor) measuring radiance simultaneously. The target sensor measured water surface radiance and the reference sensor measured radiance from reference panel. The target sensor of 8° field of view was positioned 0.3 m above water surface and 0.50 m from the side of the tank. The reference sensor had a 25° field of view and positioned over a Lambertian white reference panel (0.07 × 0.07 m) made of Barium Sulphate to provide radiance information of the incoming solar radiation. The spectro-radiometer automatically optimized the integration time for both sensors based on the sunlight conditions. The reflectance $R(\lambda)$ of the water surface was calculated using the following equation:

$$R(\lambda) = 100 \times \frac{L_T(\lambda)}{L_R(\lambda)}, \tag{2}$$

where $L_T(\lambda)$ was the wavelength-specific target radiance, and $L_R(\lambda)$ was the corresponding radiance from the reference panel.

For each suspended mineral concentrations C discussed in the subsequent section, reflectance ($R_C(\lambda)$) was measured. The reflectance ($R_m(\lambda)$) of the 0.01-m-thick layer of dry soil spread over a black surface was also obtained. The ratio of diffused light to total light ($r_D(\lambda)$) at the time of the experiment was measured. Direct light on the reference panel was blocked using a black wooden board of 0.1 m × 0.1 m at a distance of about 0.3 m from the reference panel in the direction of direct light. In this way, the light which reached the reference panel was only diffused light radiance $L_D(\lambda)$. The percentage diffused light ratio was then calculated as:

$$r_D(\lambda) = 100 \times \frac{L_D(\lambda)}{L_R(\lambda)}. \tag{3}$$

Three replications were averaged for each data collection for further analysis.

2.3 *Suspended mineral concentrations*

In the beginning, before filling water in the tank, reflectance was measured for the black surface of the tank bottom ($R_b(\lambda)$). Afterwards, the tank was filled with tap water up to the 0.75 m depth. Weighted quantities of silty loam soil (US Department of Agriculture (USDA): loamy, siliceous, subactive, thermic Lithic Dystrudepts) were sequentially added in tank water to create seven different suspended mineral concentrations of 0.24, 4.3, 24.7, 61.1, 195.2, 377.8 and 560.4 g m^{-3}, respectively. The soil samples were dried and sieved, and soil particles finer than 0.05 mm were used in this study. The suspended mineral concentrations of up to 560.4 g m^{-3} were typical of the upper limit of the suspended mineral concentrations used in earlier tank studies (300 g m^{-3} in Han *et al.* 1994; 500 g m^{-3} in Han 1997 and 1000 g m^{-3} in Lodhi *et al.* 1997). The soil sediments in the tank were kept in suspension by manually stirring at regular intervals. The data were collected using the spectro-radiometer within 20 s of sediment addition in order to minimize the amount of sediments settling at the bottom.

3. Inverse modelling approach

3.1 *Mathematical formulation of IOP of soil particles*

The molecular scattering coefficient of water $b_w(\lambda)$ are known and can be assumed to be constant over the temperature and pressure range of the experiment (Stramski *et al.* 2004). The values of $b_w(\lambda)$ and absorption coefficient, $a_w(\lambda)$ for the current study were taken from Smith and Baker (1981), which are commonly employed for remote sensing studies. However, for the wavelength range of 400–700 nm, $a_w(\lambda)$ values as reported by Pope and Fry (1997) were used due to their better reported accuracy (Stramski *et al.* 2004).

The IOPs of mineral particles are a function of wavelength and suspended sediment concentrations. For a specific wavelength λ, IOP of a suspended mineral particle at a concentration C is comprised of the absorption coefficient $a_{m\_C}(\lambda)$, total scattering coefficient $b_{m\_C}(\lambda)$ and volumetric scattering function $\beta_{m\_C}(\varphi,\lambda)$ for an angle φ, which is the angle between the propagation direction of the light beam and the direction of scatter. In addition, derived coefficients such as total attenuation coefficient $c_{m\_C}(\lambda)$, which is equal to the sum of $a_{m\_C}(\lambda)$ and $b_{m\_C}(\lambda)$, backscattering coefficient $b_{bm\_C}(\lambda)$ and backscattering ratio b_{bm_C}, which is the ratio of $b_{bm\_C}(\lambda)$ and $b_{m\_C}(\lambda)$, have also been used by the research community for defining IOPs of suspended mineral particles.

Backscattering coefficient ($b_{bm\_C}(\lambda)$) at suspended mineral concentration C is normally expressed as follows (Smith and Baker 1981, Sathyendranath *et al.* 2001, Lee *et al.* 2002, Cota *et al.* 2003):

$$b_{bm\_C}(\lambda) = b_{bm}(\lambda_0)\left(\frac{\lambda_0}{\lambda}\right)^Y C^X, \tag{4}$$

where $b_{bm}(\lambda_0)$ is the mass-specific backscattering coefficient at a reference wavelength λ_0 which was selected as 550 nm in this study, and the Y and X are the wavelength and concentration exponents, respectively.

The PHO-MC model not only required the value of the scattering coefficient but also its phase function as input. In this model, scattering phase function was characterized by the commonly used Henyey-Greenstein phase function (Prahl *et al.* 1989, Mobley 1994, Gjerstad *et al.* 2003). The value of asymmetry parameter g was assumed to be 0.9 for the

suspended mineral. It was also assumed that scattering does not have an azimuthal dependence. For the assumed value of g, the calculated value of B_{bm} (b_{bm_C} / b_{m_C}) was 0.0229. The scattering coefficient $b_{m\_C}(\lambda)$ can, thus, be calculated as follows:

$$b_{m\_C}(\lambda) = \left(\frac{b_{bm\_C}(\lambda)}{0.0229}\right). \tag{5}$$

Absorption coefficient of mineral particles ($a_{m\_C}(\lambda)$) generally decreases with increasing wavelength, and can be approximated by an exponential function (Hoepffner and Sathyendranath 1993, Pierson and Strombeck 2001, Arst 2003). Instead of assuming its variation independent from the scattering coefficients, a relationship (equation (6)) was established between $b_{bm\_C}(\lambda)$ and $a_{m\_C}(\lambda)$ using the measured values of $R_M(\lambda)$ which were the basic optical characteristics of the mineral particles used in this study.

$$R_M(\lambda) \propto \frac{b_{bm\_C}(\lambda)}{a_{mC}(\lambda) + b_{bm\_C}(\lambda)} = (\alpha)\frac{b_{bm\_C}(\lambda)}{a_{mC}(\lambda) + b_{bm\_C}(\lambda)}. \tag{6}$$

The coefficient of proportionality in this relation, α, varies depending on the illumination conditions at the time of $R_M(\lambda)$ measurement. In the current experiment, a dry soil measurement was taken only once; thus, the value of α was a unique number. However, α will be a different number for a different type of mineral particle and $R_M(\lambda)$ measurement. Generally wavelength dependence of α is weak, so it was ignored (Wozniak and Stramski 2004). Equation (7) can thus be used to estimate the value of $a_{m\_C}(\lambda)$ as:

$$a_{m\_C}(\lambda) = b_{bm\_C}(\lambda)\left[\frac{\alpha}{R_M(\lambda)} - 1\right]. \tag{7}$$

Equations (4), (5) and (7) can be used for obtaining the IOPs of the mineral particle, (i.e. $a_{m\_C}(\lambda)$, and $b_{m\_C}(\lambda)$) at any C, and λ, provided an optimal value of the four parameters, viz. $b_{bm}(550)$, Y, X and α, are known.

3.2 *Optimization approach of inverse modelling*

Reflectance data at three mineral particle concentrations (560.4, 195.2 and 24.7 g m^{-3}), out of seven different suspended mineral concentrations data collected in the water tank study, were selected for inverse modelling purposes. These three concentrations broadly represented the range of suspended mineral concentration of the study. Of the measured reflectance data between 400 and 800 nm, 11 different wavelengths (400, 475, 550, 590, 600, 625, 670, 700, 710, 750 and 775 nm) were used for inverse modelling. Therefore, a set of these 33 measured reflectances at 11 different wavelengths for each of the three mineral particle concentrations constituted the data used in inverse modelling for searching the optimal solution of the four parameters of the IOP equations.

The optimization of four parameters entails searching the entire parameter space of the four parameters $b_{bm}(550)$, Y, X and α. The optimization function used to find the solution of these four parameters was to minimize the mean sum of square error (MSE) calculated as:

$$\mathrm{MSE} = \frac{1}{NP}\sum_{n=1}^{N}\sum_{p=1}^{P}(R_M(\lambda_n) - R_S(\lambda_n))^2, \tag{8}$$

where N and P were, respectively, the number of study wavelengths (=11) and number of study mineral particle concentrations (=3) in this study; $R_M(\lambda_n)$ was the measured reflectance at wavelength λ_n and mineral particle concentration C_p; and $R_S(\lambda_n)$ was the PHO-MC model predicted reflectance at wavelength λ_n and mineral particle concentration C_p. The $R_S(\lambda_n)$ were calculated when PHO-MC model input was the calculated IOP values based on four parameters selected from the parameter space.

Evaluating MSE at one point of parameter space required approximately 5–10 h on a desktop computer (Intel Pentium 4, 2.8 GHz), as the model has to predict 33 reflectances, and 10^7 photons were used to predict each reflectance. The IOP values determined the computing time by affecting the number of scattering of a photon before it either got completely adsorbed or escaped the water surface. To overcome this computational burden of inverse modelling we used a pseudo-simulator model to reduce the time of model run and GA for searching the optimal solution in the parameter space. Figure 3 shows the flow chart of the optimization approach used. The pseudo-simulator model was used as a replacement to the PHO-MC model to interpolate model values for a given set of IOP values. The computation time for the simulator model to predict the reflectance for a set of soil IOP values was several orders of magnitude less than the time taken to make the same predictions by the actual PHO-MC model.

3.3 *Pseudo-simulator model*

At one particular wavelength, reflectance due to different sets of mineral particle IOPs when all other inputs of the PHO-MC model are the same can be interpolated by a simulator model instead of the actual PHO-MC model. A simulator model is a

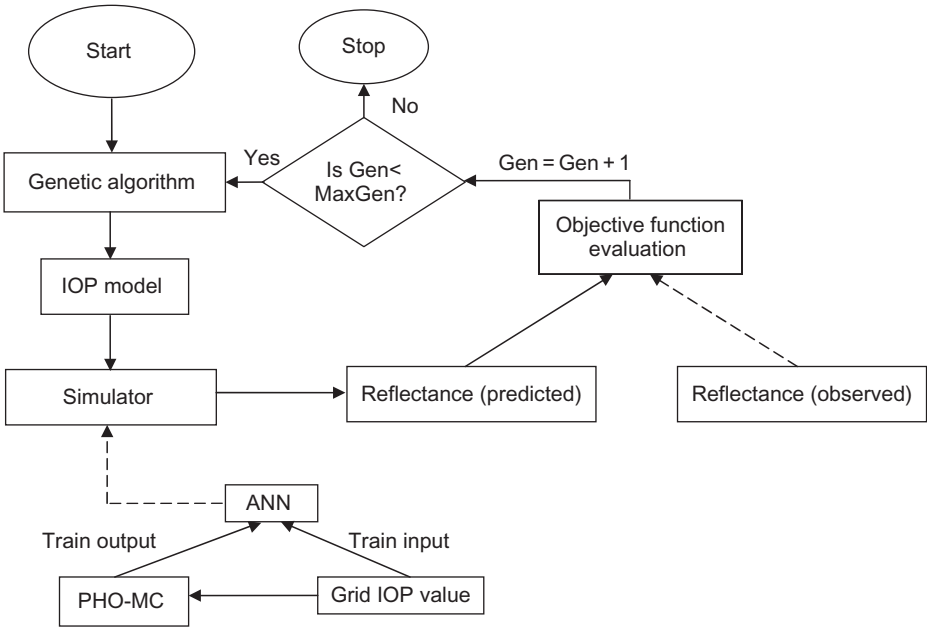

Figure 3. Flow chart of the inverse model for determination of inherent optical properties using artificial neural network as a simulator and genetic algorithm as an optimizer.

regression model developed based on two parameters of suspended mineral IOPs (a_m and b_m) as the independent variables and PHO-MC model predicted reflectance as the dependent variable. An individual simulator model was developed for each of the 11 wavelengths studied in the inverse model. Separate simulator models for each wavelength were necessary to account for the variability of water IOPs with the wavelength. A combination of 16 b_m values ranging from 0.0 to 0.296523 m^{-1} and ten a_m values ranging from 0.0 to 0.200000 m^{-1} provided 160 grid points of set of mineral particle IOP values for which the PHO-MC model was run at each of the selected 11 wavelengths.

ANN as a pseudo-simulator was used due to its ability in interpolating non-linear functions. Through learning procedures, ANNs have the ability to approximate any non-linear relationship that exists between a set of independent variables as input and their corresponding set of dependent variables as outputs. The major advantage of ANN over classical statistical approaches is that ANNs do not require the input data to have a Gaussian distribution. Many researchers have reported ANN to be more robust when input data do not follow a Gaussian distribution (Hepner *et al.* 1990, Paola and Schowengerdt 1997). Contrary to the estimates of constant and independent variables coefficients of a mathematical equation to predict dependent variables in the statistical regression model, an ANN attempts to mimic the human mental and neural structure and functions (Hsieh 1993) to develop a relationship between dependent and independent variables. The network topology consists of a set of nodes (neurons) at the input layer equal to the number of independent variables, one or more intermediate layers with hidden neurons and an output layer consisting of one or more neurons depending upon the number of dependent variables. Each node in a layer receives and processes weighted input from the previous layer and transmits its output to nodes in the following layer through links. Each link is assigned a weight, which is a numerical estimate of the connection strength. The weighted summation of inputs to a node is converted to an output according to a transfer function.

One hundred and sixty IOP values of mineral particles and corresponding PHO-MC model predicted reflectances were fed as training data to develop the ANN model. The effectiveness of the pseudo-simulator model was tested based on comparing pseudo-simulator predicted reflectances at 36 different combinations of suspended mineral IOP values and corresponding PHO-MC model predicted reflectances.

A three-layered feed-forward network (figure 4) was trained using the ANN toolbox of MATLAB (The Mathworks, Inc., Natick, MA, 2000) to obtain the weights and biases of each network. The network used a sigmoid transfer function for five hidden neurons (optimized by trial and error) and one output neuron. Sigmoid function requires values between zero and one, therefore input and output data sets were standardized by scaling the values between 0 and 1. The supervised training was accomplished with the help of a back-propagation algorithm (Levenberg–Marquardt) as implemented in MATLAB. Twenty-one parameters of a trained neural network could be used to calculate the value of output reflectance based on given input values of mineral IOP (equation (9)). This equation served as the pseudo-simulator of the PHO-MC model.

$$\overline{O} = f\left(\left(\sum_{i=1}^{5}(f((aWA(i)+bWB(i))+bH(i)))WH(i)\right)+bO(1)\right), \qquad (9)$$

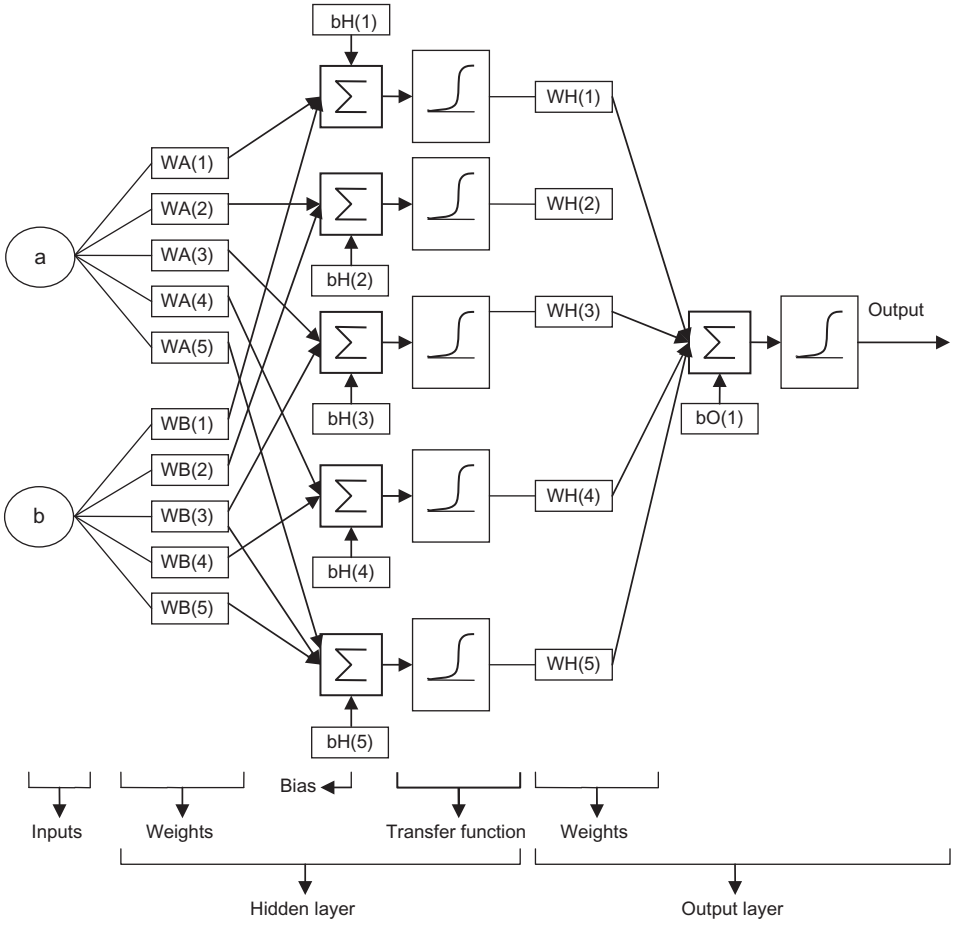

Figure 4. Artificial neural network (feed forward) structure used in this study as a pseudo simulator.

where O was the output reflectance for the mineral particle IOP values a and b. Refer to figure 4 for the nomenclature of weights and bias values. Sigmoid function $f(.)$ was given by:

$$f(x) = \frac{1}{1 + e^{-x}}. \tag{10}$$

3.4 *Optimization algorithm*

The optimization model helped to intelligently select the next set of four parameters of the mineral particle IOP equations based on the results of the previous set of four parameter performances instead of randomly selecting the next set of four parameters values. The Nondominated Sorted Genetic Algorithm-II (NSGA II) (Deb 2001, Deb *et al.* 2002) was used for the optimization of the four parameters of IOP equation in this study. GA uses the concepts of evolution of the objective functions where the variables undergo mutation and crossover of the population (entities) in each

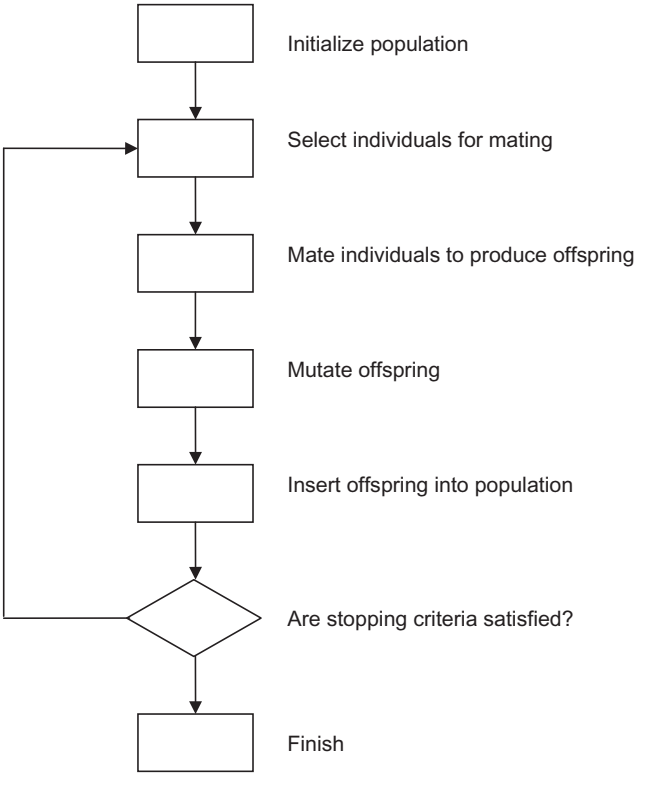

Figure 5. Typical flow chart of a genetic algorithm operation.

generation until it completes the required number of generations (figure 5). In GA, probabilistic transition rules instead of deterministic rules determine the specific best solution. Though randomized, GA is not a simple random walk. It efficiently exploits historical information on objective function values to speculate on new search points with expected improved performance. GAs generally perform well in large and complex search spaces and, when properly implemented, are capable of both exploration (broad search) and exploitation (local search) of the search space (Goldberg 1989). The most important feature of GAs is their robust nature and the balance between efficiency and efficacy necessary for survival in many different environments.

4. Result and discussion

The R_M for the dry soil increased from its lowest value (5.21%) at 400 nm wavelength to its maximum value of 35.6% at 800 nm (figure 6). The average value of the ratio of diffused light to the total light decreased as the wavelength increased (figure 7). Based on these inputs, the PHO-MC model reflectances were predicted at 160 different combinations of a_m and b_m values at each of the 11 wavelengths used in this study. Figure 8 shows the variation in PHO-MC predicted reflectance at four selected wavelengths of 400, 550, 700 and 775 nm where water absorption properties differed substantially. As expected the reflectance increased as the value of a_m decreased or b_m increased. For the same a_m and b_m values, reflectance was different for different

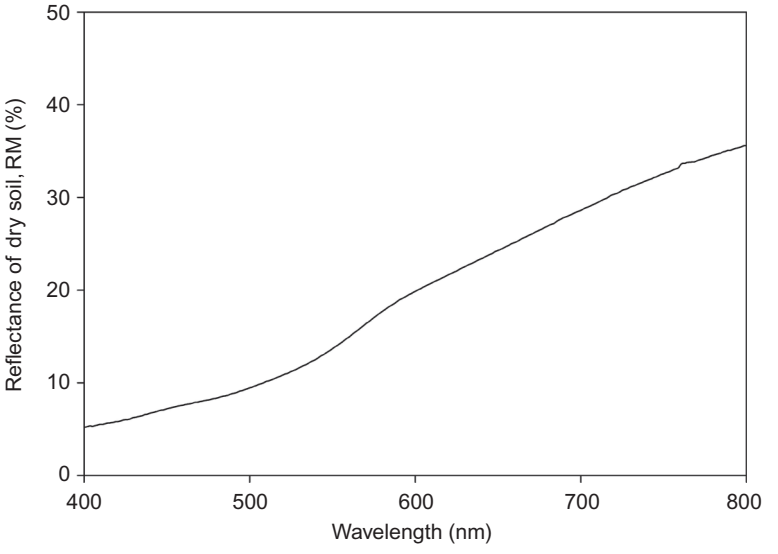

Figure 6. Reflectance ($R_M(\lambda)$) of a 0.01-m-thick layer of dry soil spread over a black surface.

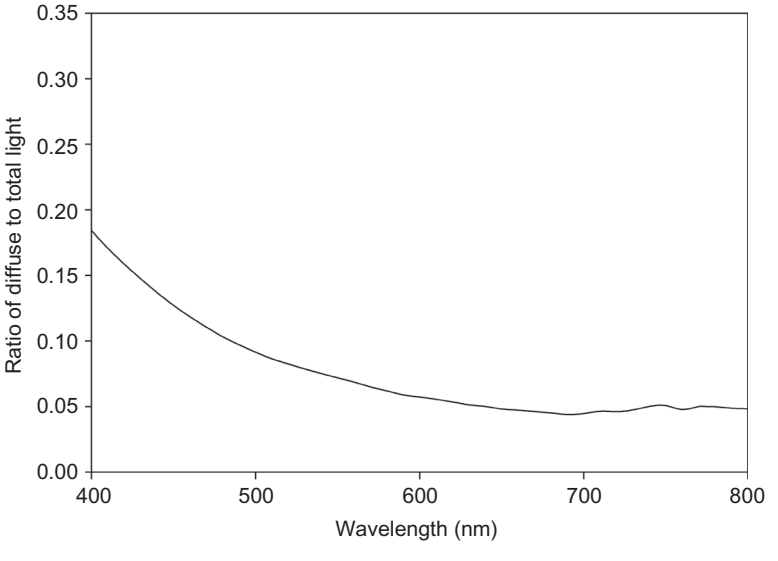

Figure 7. Average value of the ratio of diffused radiance to the total downwelling radiance during the experiment.

wavelength sets. It was higher for the 400 nm wavelength where overall water absorption was less, and scattering was more. Water absorption increased, and scattering decreased as the wavelength increased, and therefore reflectance decreased for the sets of higher wavelength.

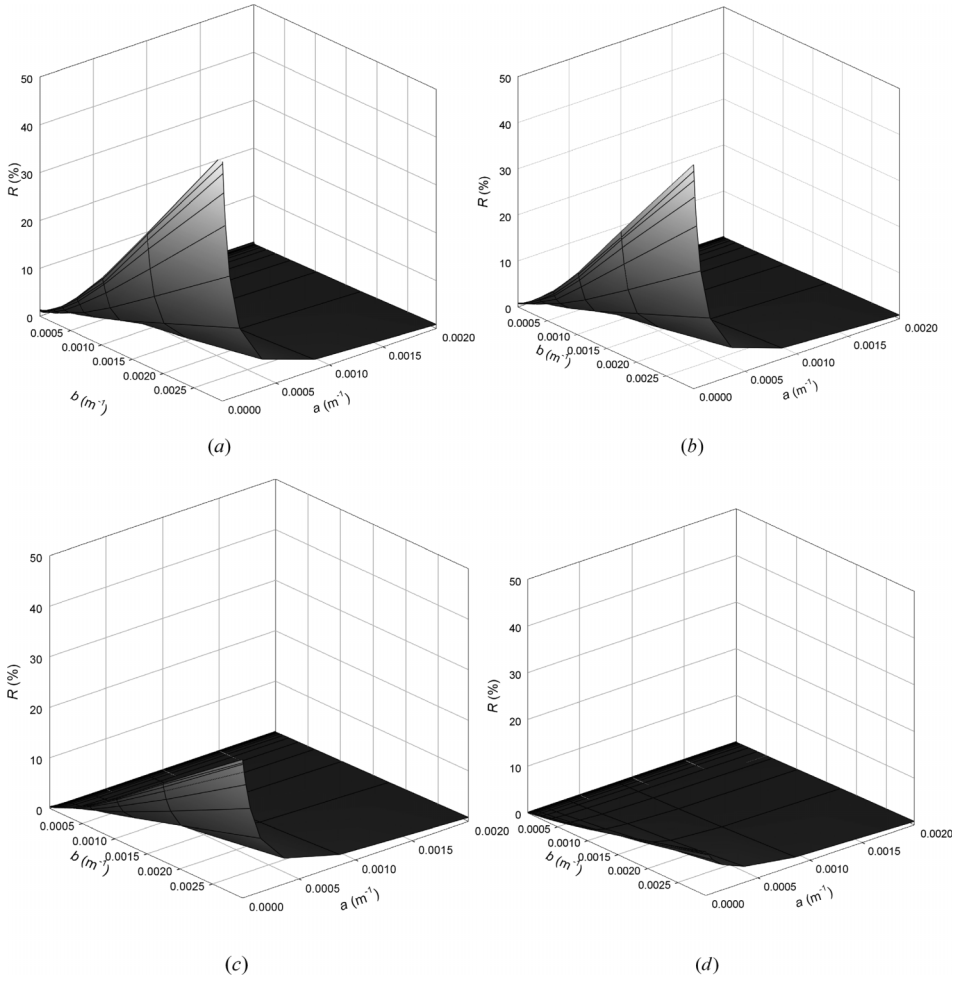

Figure 8. Simulated values of reflectance using PHO-MC model 400 nm wavelength (*a*), 550 nm wavelength (*b*), 700 nm wavelength (*c*) and 775 nm wavelength (*d*).

4.1 *Pseudo-simulator model performance*

Pseudo-simulators at each of the 11 wavelengths of the inverse modelling performed well. The coefficient of determination between the predicted reflectance values of pseudo-simulator and predicted reflectance values of PHO-MC model at all 160 sets of a_m and b_m combinations of calibration data set was more than 0.99 (table 2). The pseudo-simulator performance at the validation point was also comparable ($r^2 >$ 0.98) to the calibration data set (table 2).

To generate grid point values of reflectance at selected 160 combinations of a_m and b_m values, the PHO-MC model took 20–27 h on a desktop computer for the wavelengths used in this study. The maximum and minimum time of the run was at 400 nm and 800 nm wavelengths, respectively. The total time to run PHO-MC model for the training data set of all 11 wavelength was about 275 h. Based on the average

Table 2. Coefficient of determination (R^2) for the ANN model at different wavelength to simulate the PHO-MC predicated reflectance based on a training data set of 160 combinations of a_m and b_m values.

	Coefficient of determination (R^2) between PHO-MC model predicted reflectance and ANN model regressed values	
Wavelength (nm)	Training data set	Validation data set
400	0.9999	0.9998
475	0.9999	0.9999
550	0.9999	0.9996
590	0.9999	0.9997
600	0.9999	0.9999
625	0.9999	0.9996
675	0.9999	0.9998
700	0.9999	0.9985
710	0.9999	0.9998
750	0.9997	0.9991
775	0.9997	0.9824

of these timings, if the actual PHO-MC model was run to simulate 33 reflectances to check error for one set of parameters for IOP determination, the desktop PC time would have been approximately 6 h. Therefore, examination of entire space of all four parameters ($b_{bm}(550)$, Y, X and α) even at discrete 10^{12} points (total permutations of four parameters assuming only 10^3 discrete values for each parameter) would need more than 10^8 years of computational time using to run the original PHO-MC model.

Since the optimization process by GA involved 20 000 sets (100 populations $\times$ 200 generation) to run during its search for the global optima of the parameters, the computer time required would have been 120 000 h (>13.7 years). However, due to the use of ANN simulator models in the GA instead of the actual PHO-MC model, run time was reduced to 9 min.

4.2 *Genetic algorithm performance*

The error propagation of the objective function with the generation is depicted in figure 9. It can be said that the parameters of the IOP equations identified in successive generations were, on average, better (less MSE) than the previous generations. It showed that the GA was capable of learning from previous results of MSE of the parameter values and selected a better set of parameters in the next generation.

4.3 *Inverse model values of IOP*

The optimized values of the parameters $b_{bm}(550)$, Y, X and α were 0.0035 $m^2\ g^{-1}$, 0.1254, 0.7505 and 1.0670, respectively. The corresponding objective function value (MSE) was 0.0122. Coefficient Y, which determines the variation of scattering coefficient with wavelength, was a value near zero (0.1254) indicating that the scattering coefficient variation with wavelength was less. This observation was similar to results reported by Hamre *et al.* (2003) who found that the scattering coefficient did not vary

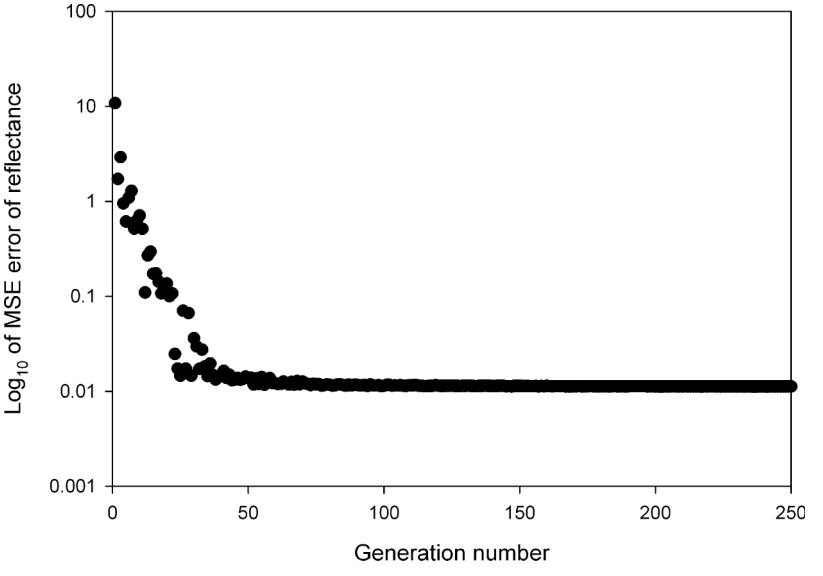

Figure 9. Mean square error (MSE) of predicted versus measured reflectance as the number of generation proceeds in genetic algorithm optimization.

much with wavelength when the particle size was more than 7 μm. Kopelevich (1983) and Kopelevich and Mezhericher (1983) found that Y decreased to 0.3 from 1.7 when the particle size increased from less than 1 μm to more than 1 μm. For the measurement of the optical properties of the Asian dust, Stramski *et al.* (2004) found that samples with relatively large particles were characterized by a weaker dependence of scattering on the wavelength.

The optimized value (0.0035 $m^2\ g^{-1}$) of $b_{bm}(550)$ was less than the lower range of the reported backscattering coefficient range reported by Arst (2003) based on a compilation of three different studies (0.02–0.10 $m^2\ g^{-1}$). In this study, exponent X for the concentration was found to be 0.7505, which was similar to the value reported for chlorophyll scattering (0.62 by Morel (1980), Gordon and Morel (1983) and Morel and Maritorena (2001); 0.766 by Loisel and Morel (1998)). Based on the parameters optimized, figure 10 shows the mass specific absorption coefficient for the mineral particles made up from silt loam soil (USDA: loamy, siliceous, subactive, thermic Lithic Dystrudepts). The calculated value of mass specific absorption coefficient at 443 nm was 0.054 $m^2\ g^{-1}$, which was within the range of 0.03 to 0.1 $m^2\ g^{-1}$ of the mass specific absorption coefficient at 443 nm reported by Babin and Stramski (2004) from 24 samples. This value of mass-specific absorption coefficient at 443 nm was also consistent with the values reported for different coastal waters around Europe, where the no-algal particulate absorption at 443 nm normalized to the dry mass of particle ranged between 0.033 and 0.067 $m^2\ g^{-1}$ (Babin *et al.* 2003, table 5). The calculated value (0.071 $m^2\ g^{-1}$) of mass-specific absorption coefficient at 400 nm (figure 10) is also consistent with the measurement of a dust sample's mass specific absorption coefficient by Stramski *et al.* (2004) at 400 nm, which varied from 0.028 for the soil dust from the Chinese desert near Dunhuang to 0.15 for the soil dust of volcanic origin in the Cheju Island (South Korea).

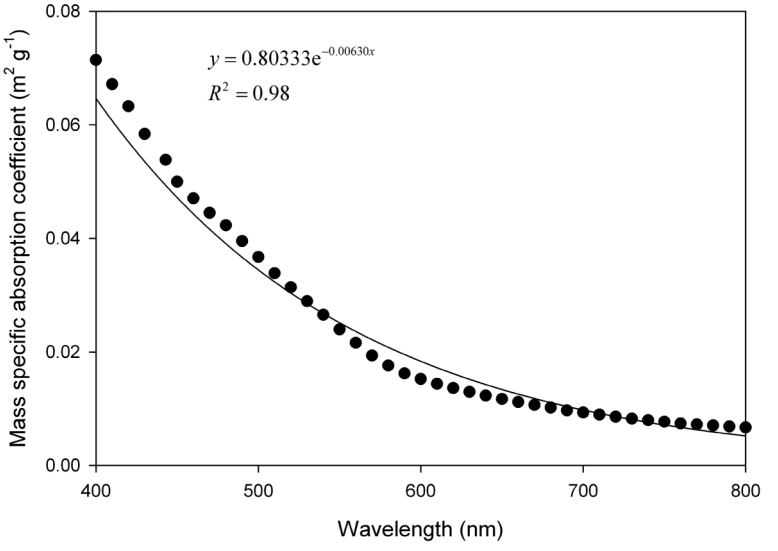

Figure 10. Spectra of the mass-specific absorption coefficient based on the optimized parameter from the tank study for the Silty loam soil (USDA: loamy, siliceous, subactive, thermic Lithic Dystrudepts).

Relative sensitivity analysis (S_r) of each parameter was calculated as:

$$S_r = \frac{P}{O}\frac{(O_2 - O_1)}{(P_2 - P_1)}, \tag{11}$$

where P and O are the base value of input and output. The base value of each parameter was changed by ±5% from its optimum value keeping all other three parameters constant at their optimum value to get P_1 and P_2 and the corresponding O_1 and O_2. The outputs considered were the mean sum of square error which was the objective function of the GA and average value of the predicted reflectance (table 3). The exponent of the concentration X was found to be the most sensitive parameter. The high sensitivity of X indicates that the PHO-MC model ability to differentiate concentration based on the change in the reflectance value is high. Parameter α was found to be the second most sensitive parameter followed by $b_{bm}(550)$. Exponent Y was not found to be a sensitive parameter, indicating that an error in determination of this parameter should cause a relatively small error in the modelling of reflectance.

Table 3. Relative sensitivity of the parameters of the equations used to estimate the IOP of suspended sediment (equations (4), (5) and (7)).

	Relative sensitivity for the output	
Parameter	Reflectance	Sum of error
$b_{bm}(550)$	0.37	1.21
Y	0.00	0.00
X	2.00	–14.56
α	–0.71	–1.91

These optimized values of $b_{bm}(550)$, Y, X and α were then validated by calculating IOPs for an independent validation data set of suspended sediment concentrations and wavelengths and then forward modelling to predict reflectance values from the PHO-MC model to compare with the observed reflectance values. A data set of 287 value of seven studied concentrations of suspended minerals and 41 wavelengths λ_n ($n = 1, 2, \ldots 41$), 10 nm apart, in the 400–800 nm range was used for the validation. Because pseudo-simulator developed was wavelength-specific, those could not be used for these 41 wavelengths selected for the validation. Therefore, the actual PHO-MC model was run for calculating reflectance values at validation points. Figure 11 depicts the observed reflectances and predicted reflectances. The simulated reflectance values followed the trend at all the wavelengths and concentrations (figure 11). A highly significant Pearson product-moment correlation coefficient ($r = 0.99$, $p < 0.01$) was found between the predicted and measured reflectances. The MSE of the validation was 0.033, which was low and comparable with the MSE for the calibration (0.012), indicating a good validation of the IOP model results. Good performance of the validation exercise illustrated the effectiveness of the inverse modelling approach of this study. A significant correlation between simulated and measured remote sensing reflectance for the 287 points of the test shows that the inverse modelling approach used here can provide an accurate estimate of suspended sediments IOP values which can be subsequently used for forward modelling of PHO-MC to accurately predict reflectance at different wavelengths and concentrations of the mineral particles.

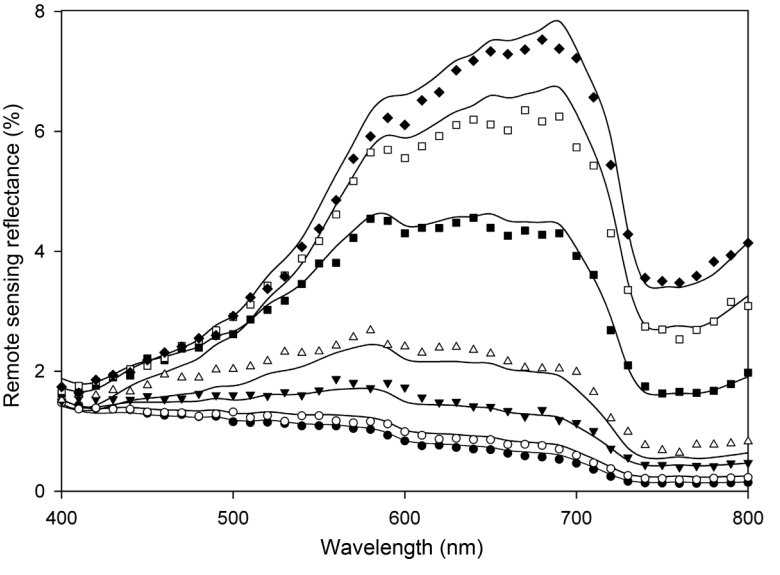

Figure 11. Measured (solid lines) and simulated (dotted points) remote sensing reflectance of water with soil concentrations of 0.24, 4.3, 24.7, 61.1, 195.2, 377.8 and 560.4 g m^{-3}, respectively, in the water tank experiment. Reflectance has increased as the soil concentration has increased. The lowest curve shows the value for the lowest soil concentration (0.24 g m^{-3}), and the highest curve shows the value for the highest concentration (560.4 g m^{-3}).

5. Summary and conclusions

An inverse modelling approach is presented to calculate the inherent optical properties of suspended sediments using a PHO-MC model in a tank study. This approach is significantly different from other inverse modelling approaches which used simple semi-analytical models only. These semi-analytical models are not only an approximation of the actual radiative transfer equation but also have limitation to be applicable to only infinitely deep water bodies. The approach presented here used a physical model (PHO-MC) which can account for different water depths, bottom reflectances, sun angles and lighting conditions. Estimated computation time to find optimized values of IOP parameters was reduced by several orders of magnitude by using the pseudo-simulator model in place of the actual PHO-MC model and reducing the number of searches required by the optimization technique of NSGA II. A wavelength-specific Artificial Neural Network was used as pseudo-simulator. The advanced optimization technique of NSGA II required only 200 000 runs for optimization of parameter values compared with a 10^{12} run for searching the entire parameter space.

Suspended sediments IOP variation with wavelengths and sediment concentrations was parameterized with four parameters. Mean sum error between the PHO-MC model predicted reflectance to measured reflectance values above the water surface in a tank study for 33 combinations of 11 wavelengths and three suspended sediment concentrations decreased to 0.0122 for optimal IOP parameter values. The determined IOP values of suspended sediment were validated by predicting 287 reflectances for an independent set of different wavelengths and sediment concentrations values with a mean square error of 0.03. A highly significant Pearson product-moment correlation coefficient ($r = 0.99$, $p < 0.01$) was found between predicted reflectance values and correspondingly measured reflectance values for the validation data set. The inverse modelling approach developed in this study should be applicable to any remote sensing model to predict reflectance based on wavelength and IOP values.

Acknowledgements

This study was funded by US Environmental Protection Agency (X7-97654601-0) and the USDA-CSREES through the Regional Research Project (S-1042: Modeling for TMDL development, and watershed based planning, management and assessment). We thank Dr Sreekala G. Bajwa for providing spectroradiometer for experimental data collection. Comments by Dr K. P. Sudheer and two anonymous reviewers improved the initial version of this manuscript.

References

Aas, E., 1987, Two-stream irradiance model for deep waters. *Applied Optics*, **26**, pp. 2095–2101.

Arst, K.I., 2003, *Optical Properties and Remote Sensing of Multicomponental Water Bodies* (New York: Springer).

Babin, M., Morel, A., Fournier-Sicre, V., Fell, F. and Stramski, D., 2003, Light scattering properties of marine particles in coastal and open ocean waters as related to the particle mass concentration. *Limnology and Oceanography*, **48**, pp. 843–859.

Babin, M. and Stramski, D., 2002, Light absorption by aquatic particles in the near-infrared spectral region. *Limnology and Oceanography*, **47**, pp. 911–915.

Babin, M. and Stramski, D., 2004, Variations in the mass-specific absorption coefficient of mineral particles suspended in water. *Limnology and Oceanography*, **49**, pp. 756–767.

Barnard, A.H., Zaneveld, J.R.V. and Pegau, W.S., 1999, In situ determination of the remotely sensed reflectance and the absorption coefficient: closure and inversion. *Applied Optics*, **38**, pp. 5108–5117.

Baruah, P.J., 2000, Application of remote sensing and smart algorithms for modeling of water quality in Lake Kasumigaura. PhD dissertation, University of Tsukuba, pp. 154.

Ciotti, A.M., Lewis, M.R. and Cullen, J.J., 2002, Assessment of the relationships between dominant cell size in natural phytoplankton communities and the spectral shape of the absorption coefficient. *Limnology and Oceanography*, **47**, pp. 404–417.

Cota, G.F., Harrison, W.G., Platt, T., Sathyendranath, S. and Stuart, V., 2003, Bio-optical properties of the Labrador Sea. *Journal of Geophysical Research – Oceans*, **108**, pp. 1–14 .

Deb, K., 2001, *Multi-Objective Optimization Using Evolutionary Algorithms* (Hoboken, NJ: Wiley).

Deb, K., Pratap, A., Agarwal, S. and Meyarivan, T., 2002, A fast and elitest multiobjective genetic algorithm, NSGA-II. *IEEE Transactions on Evolutionary Computation*, pp. 182–197.

Doyle, J.P. and Rief, H., 1998, Photon transport in three-dimensional structures treated by random walk techniques. Monte Carlo benchmark of ocean colour simulations. *Mathematics and Computers in Simulation*, **47**, pp. 215–241.

Garg, V., 2006, Development and evaluation of a physical hyperspectral optical – Monte Carlo model for an aquatic medium reflectance simulation. PhD thesis, University of Arkansas.

Garg, V., Chaubey, I. and Singh, S., 2009, Evaluation of a hyperspectral optical – Monte Carlo remote sensing model in a water tank study. *Transactions of the American Society of Agricultural and Biological Engineers*, **52**, pp. 1347–1353.

Gimond, M., 2002, Development and sensitivity analyses of a hyperspectral optical Monte Carlo model for coastal and estuarine water quality applications. PhD thesis, Florida Institute of Technology.

Gjerstad, K.I., Stamnes, J.J., Hamre, B., Lotsberg, J.K., Yan, B. and Stamnes, K., 2003, Monte Carlo and discrete-ordinate simulations of irradiances in the coupled atmosphere–ocean system. *Applied Optics*, **42**, pp. 2609–2622.

Goldberg, D.E., 1989, *Genetic Algorithm in Searching, Optimization, and Machine Learning* (Reading, MA: Addison-Wesley-Longman).

Gordon, H.R., Brown, O.B. and Jacobs, M.M., 1975, Computed relationships between the inherent and apparent optical properties of a flat homogeneous ocean. *Applied Optics*, **14**, pp. 417–427.

Gordon, H.R. and Morel, A., 1983, Remote assessment of ocean color for interpretation of satellite visible imagery: a review. In *Lecture Notes on Coastal and Estuarine Studies*, R.T. Barber, C.N.K. Mooers, M.J. Bowman and B. Zeizschel (Eds), pp. 1–114 (New York: Springer).

Gordon, H.R. and Boynton, G.C., 1997, Radiance–irradiance inversion algorithm for estimating the absorption and backscattering coefficients of natural waters: Homogeneous waters. *Applied Optics*, **36**, pp. 2636–2641.

Hamre, B., Frette, O., Erga, S.R., Stamnes, J.J. and Stamnes, K., 2003, Parameterization and analysis of the optical absorption and scattering coefficients in a western Norwegian fjord: a case II water study. *Applied Optics*, **42**, pp. 883–892.

Han, L., 1997, Spectral reflectance with varying suspended sediment concentrations in clear and algae-laden waters. *Photogrammetric Engineering and Remote Sensing*, **63**, pp. 701–705.

Han, L., Rundquist, D.C., Liu, L.L., Fraser, R.N. and Schalles, J.F., 1994, The spectral responses of algal chlorophyll in water with varying levels of suspended sediment. *International Journal of Remote Sensing*, **15**, pp. 3707–3718.

Hepner, G., Logan, T., Ritter., N and Bryant, N., 1990. Artificial neural network classification using a minimal training set – comparison to conventional supervised classification. *Photogrammetric Engineering and Remote Sensing*, **56**, pp. 469–473.

Hoepffner, N. and Sathyendranath, S., 1993, Determination of the major groups of phytoplankton pigments from the absorption spectra of total particulate matter. *Journal of Geophysical Research – Oceans*, **98**, pp. 22789–22803.

Hsieh, C., 1993, Some potential applications of artificial neural networks in financial management. *Journal of Systems Management*, **44**, p. 15.

Keiner, L.E. and Yan, X.H., 1998, A neural network model for estimating sea surface chlorophyll and sediments from thematic mapper imagery. *Remote Sensing of Environment*, **66**, pp. 153–165.

Kirk, J.T.O., 1984, Dependence of relationship between inherent and apparent optical properties of water on solar altitude. *Limnology and Oceanography*, **29**, pp. 350–356.

Kopelevich, O.V., 1983, Small-parameter model of optical properties of sea water. In *Ocean Optics, vol 1: Physical Ocean Optics*, A.S. Monin, (Ed.) (Moscow: Nauka Publications), [in Russian].

Kopelevich, O.V. and Mezhericher, E.M., 1983, Calculation of spectral characteristics of light scattering by sea water. *Izvestiya Atmospheric and Oceanic Physics*, **19**, pp. 144–148.

Lee, Z.P. and Carder, K.L., 2004, Absorption spectrum of phytoplankton pigments derived from hyperspectral remote-sensing reflectance. *Remote Sensing of Environment*, **89**, pp. 361–368.

Lee, Z.P., Carder, K.L. and Arnone, R.A., 2002, Deriving inherent optical properties from water color: A multiband quasi-analytical algorithm for optically deep waters. *Applied Optics*, **41**, pp. 5755–5772.

Lodhi, M.A., Rundquist, D.C., Han, L. and Kuzila, M.S., 1997, The potential for remote sensing of loess soils suspended in surface waters. *Journal of the American Water Resources Association*, **33**, pp. 117.

Loisel, H. and Morel, A., 1998, Light scattering and chlorophyll concentration in case 1 waters: A reexamination. *Limnology and Oceanography*, **43**, pp. 847–858.

Loisel, H. and Stramski, D., 2000, Estimation of the inherent optical properties of natural waters from the irradiance attenuation coefficient and reflectance in the presence of Raman scattering. *Applied Optics*, **39**, pp. 3001–3011.

Loisel, H., Stramski, D., Mitchell, B.G., Fell, F., Fournier-Sicre, V., Lemasle, B. and Babin, M., 2001, Comparison of the ocean inherent optical properties obtained from measurements and inverse modeling. *Applied Optics*, **40**, pp. 2384–2397.

McCluney, W.R., 1976, Remote measurement of water color. *Remote Sensing of Environment* **5**, pp. 3–33.

McKee, D., Cunningham, A. and Craig, S., 2003, Estimation of absorption and backscattering coefficients from *in situ* radiometric measurements: Theory and validation in Case II waters. *Applied Optics*, **42**, pp. 2804–2810.

Mobley, C.D., 1994, *Light and Water: Radiative Transfer in Natural Waters* (San Diego: Academic Press).

Mobley, C.D., Gentili, B., Gordon, H.R., Jin, Z.H., Kattawar, G.W., Morel, A., Reinersman, P., Stamnes, K. and Stavn, R.H., 1993, Comparison of numerical-models for computing underwater light fields. *Applied Optics*, **32**, pp. 7484–7504.

Morel, A., 1980, In-water and remote measurements of ocean color. *Boundary-Layer Meteorology*, **18**, pp. 177–201.

Morel, A. and Prieur, L., 1977, Analysis of variations in ocean color. *Limnology and Oceanography*, **22**, pp. 709–722.

Morel, A. and Maritorena, S., 2001, Bio-optical properties of oceanic waters: A reappraisal. *Journal of Geophysical Research – Oceans*, **106**, pp. 7163–7180.

Panda, S.S., Garg, V. and Chaubey, I., 2004, Artificial neural networks application in lake water quality estimation using satellite imagery. *Journal of Environmental Informatics*, **4**, pp. 65–74.

PAOLA, J.D. and SCHOWENGERDT, R.A., 1997, The effect of neural-network structure on a multispectral land-use/land-cover classification. *Photogrammetric Engineering and Remote Sensing*, **63**, pp. 535–544.

PIERSON, D.C. and STROMBECK, N., 2001, Estimation of radiance reflectance and the concentrations of optically active substances in Lake Malaren, Sweden, based on direct and inverse solutions of a simple model. *Science of Total Environment*, **268**, pp. 171–188.

POPE, R.M. and FRY, E.S., 1997, Absorption spectrum 380–700 nm of pure water. II. Integrating cavity measurements. *Applied Optics*, **36**, pp. 8710–8723.

PRAHL, S.A., KEIJZER, M., JACQUES, S.L. and WELCH, J.,A., 1989, A Monte Carlo model of light propagation in tissue. In *SPIE Proceedings of Dosimetry of Laser Radiation in Medicine and Biology,* pp. 102–111.

RISOVIC, D., 2002, Effect of suspended particulate-size distribution on the backscattering ratio in the remote sensing of seawater. *Applied Optics*, **41**, pp. 7092–7101.

SATHYENDRANATH, S., COTA, G., STRUAT, V., MAASS, H. and PLATT, T., 2001, Remote sensing of phytoplankton pigments: a comparison of empirical and theoretical approaches. *International Journal of Remote Sensing*, **22**, pp. 249–273.

SATHYENDRANATH, S., LAZZARA, L. and PRIEUR, L., 1987, Variations in the spectral values of specific absorption of phytoplankton. *Limnology and Oceanography*, **32**, pp. 403–415.

SMITH, R.C. and BAKER, K.S., 1981, Optical properties of the clearest natural waters 200–800 nm. *Applied Optics*, **20**, pp. 177–184.

STRAMSKA, M., STRAMSKI, D., MITCHELL, B.G. and MOBLEY, C.D., 2000, Estimation of the absorption and backscattering coefficients from in-water radiometric measurements. *Limnology and Oceanography*, **45**, pp. 628–641.

STRAMSKI, D., BRICAUD, A. and MOREL, A., 2001, Modeling the inherent optical properties of the ocean based on the detailed composition of the planktonic community. *Applied Optics*, **40**, pp. 2929–2945.

STRAMSKI, D., BOSS, E., BOGUCKI, D. and VOSS, K.J., 2004, The role of seawater constituents in light backscattering in the ocean. *Progress in Oceanography*, **61**, pp. 27–56.

WOZNIAK, S.B. and STRAMSKI, D., 2004, Modeling the optical properties of mineral particles suspended in seawater and their influence on ocean reflectance and chlorophyll estimation from remote sensing algorithms. *Applied Optics*, **43**, pp. 3489–3503.

YACOBI, Y.Z., GITELSON, A. and MAYO, M., 1995, Remote-sensing of chlorophyll in Lake Kinneret using high-spectral-resolution radiometer and Landsat TM: spectral features of reflectance and algorithm development. *Journal of Plankton Research*, **1**7, pp. 2155–2173.